JOC The Journal of Organic Chemistry

Article

pubs.acs.org/joc

Synthesis, Structure, and Binding Properties of Lipophilic Cavitands Based on a Calix[4]pyrrole-Resorcinarene Hybrid Scaffold

Albano Galán,[†] Eduardo C. Escudero-Adán,[‡] Antonio Frontera,[∥] and Pablo Ballester*[,†,§]

[†]Institute of Chemical Research of Catalonia (ICIQ) and [‡]X-ray Diffraction Unit, ICIQ, Avgda. Països Catalans 16, 43007 Tarragona, Spain

[§]Catalan Institution for Research and Advanced Studies (ICREA), Passeig Lluís Companys, 23, 08010 Barcelona, Spain

[∥]Departament de Química, Universitat de les Illes Balears, Crta. Valldemossa Km. 7.5, 07122 Palma, Spain

Supporting Information

ABSTRACT: We report the synthesis, structural characterization, and binding properties of a series of unprecedented cavitands based on a *meso*-dodecyl-calix[4]pyrrole-resorcin[4]arene hybrid scaffold. The reported structural and conformational features of the prepared cavitands are derived from results obtained in solution, solid state, and molecular modeling studies. In the solid state, these cavitands are exclusively observed in the kite C_4 structure and as a racemic mixture of two cyclochiral conformers, which are interconverting fast on the ^{1}H NMR time scale, according to solution studies. In agreement, molecular modeling studies assign an energy preference for the kite conformer of the cavitands. The polar interior of the synthesized containers allows for the inclusion of a series of pyridine *N*-oxide derivatives. This results in the formation of 1:1 complexes that are kinetically and thermodynamically highly stable. The putative switching process between the vase and kite forms of these cavitands is investigated in solution by means of variable temperature ^{1}H NMR experiments. *N*-Oxide guests that are size and shape complementary to the volume of the cavity of the vase form are also employed to facilitate its emergence. All of the results obtained indicate the existence of a remarkable preference toward the kite conformation both in free and bound calix[4]pyrrole-based cavitands.

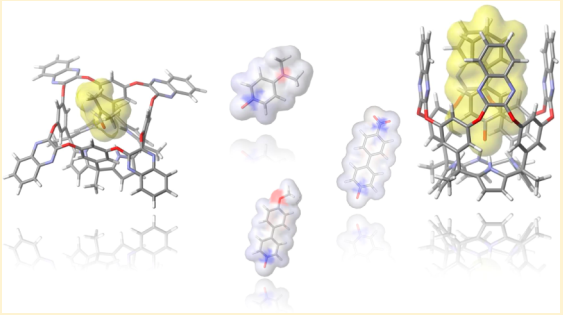

INTRODUCTION

Cavitands are synthetic molecules that contain an intrinsic cavity capable of including sizable guests (molecules or ions).[1] In this sense, the elaboration of the shallow cavity provided by the cone conformer of resorcin[4]arene **1** through the incorporation of aromatic panels at its upper rim constitutes a valuable synthetic strategy for the construction of deep cavitands.[1−4] The upper rim functionalization of **1** is easily accessible synthetically due to the presence of the eight hydroxyl groups. The construction of deeper cavities has the dual effect of increasing the shielding of bound guests from the solvent and restricting the conformational flexibility of the initial resorcinarene scaffold. In addition, extending the cavity of a receptor molecule may confer new binding properties or modulate its kinetic and thermodynamic binding features.[5] Examples of functional deep cavitands based on multiply bridged resorcin[4]arene structures are abundant in literature.[6] These compounds have been extremely useful both in the self-assembly of molecular capsules[7,8] and in the construction of covalent cages.[9] Supramolecular sensors,[10] catalysts,[11] or even molecular grippers[12,13] have also been derived from resorcinarene-based cavitands. Unfortunately, the extensive use of aromatic panels to shape and elaborate the cavity in resorcinarene-based deep cavitands renders their interiors deprived from polar functional groups. Nevertheless, attempts to functionalize the interiors of resorcinarene-based deep cavitands with one carboxylic group[14−16] or several pyrrole units[17] have been reported.

Calix[4]pyrroles are tetrapyrrolic macrocyclic compounds known to act as effective receptors for anions and electron-rich neutral compounds.[18] The substitution at each of the four *meso* positions of the calix[4]pyrrole core by a phenyl group affords aryl-extended calix[4]pyrroles containing deep cavities defined by fixed aromatic walls.[19] In 2007, our group reported the synthesis of the *α,α,α,α*-isomer of aryl-extended calix[4]pyrrole **2a** decorated with eight hydroxyl groups at its upper rim (Figure 1).[20] The structure of **2a** reminded us of resorcinarene **1** and was described as a resorcinarene-calix[4]pyrrole hybrid. We envisioned that calix[4]pyrrole-resorcinarene hybrid **2a** could be a suitable scaffold for the construction of deep cavitands functionalized with four pyrrole units at their closed ends. Our expectations were that the synthetic strategies used in the preparation of deep cavitands derived from resorcin[4]-arene **1** could be directly applied to further elaborate the aromatic cavity of **2**. Most of these synthetic strategies involved the bridging of vicinal hydroxyl groups at the upper rim with suitable aromatic spacers. To the best of our knowledge, there

Received: March 28, 2014
Published: May 20, 2014

   dx.doi.org/10.1021/jo5007224 | J. Org. Chem. 2014, 79, 5545−5557

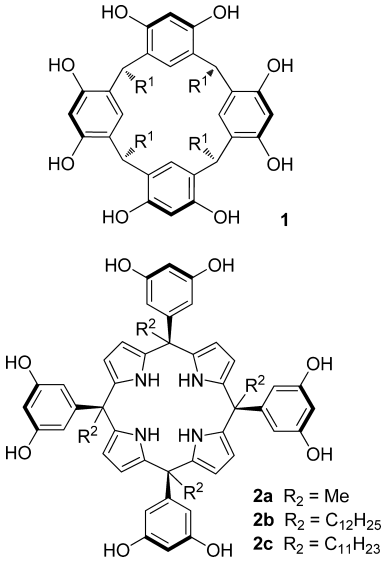

Figure 1. Molecular structures of resorcin[4]arene **1** and calix[4]-pyrrole-resorcin[4]arene hybrid **2**.

is only one example of cavitands derived from aryl-extended calix[4]pyrrole scaffolds in literature.[21] However, the described compounds do not qualify as deep cavitands. Their structures correspond to doubly bridged phosphonated cavitands derived from a tetraol aryl extended calix[4]pyrrole. These compounds are reminiscent of the phosphonate-calix[4]arene cavitands of Dalcanale[22−24] and Dutasta.[25,26] Here, we describe the synthesis of a series of tetrabridged deep cavitands derived from calix[4]pyrrole hybrid **2b**. We also report the conformational properties of the synthesized cavitands, both in solution and in solid state. Finally, we discuss the experimental results of the binding studies of these novel cavitands with pyridine *N*-oxide derivatives.

RESULTS AND DISCUSSION

Synthesis of Lipophilic Calix[4]pyrrole-Resorcin[4]-arene Hybrid 2b. All synthetic attempts to elongate the cavity of built-in calix[4]pyrrole **2a** led to reaction mixtures with low solubility in most common organic solvents. The limited solubility of the crude reaction product made the analysis of the mixture and its purification troublesome. To overcome this limitation, we decided to use the more lipophilic calix[4]pyrrole derivative **2b** as the initial building block. Calix[4]pyrrole **2b** is a structural analogue to **2c** but contains an extra carbon atom in its *meso*-alkyl chains. A synthetic procedure for calix[4]pyrrole **2c** was recently reported by Cohen.[27] Inspired by the reported synthetic methodology, we prepared dodecyl-3,5-dihydroxy-phenyl ketone **6** in 3 steps. The nucleophilic addition of dodecyl magnesium bromide to 3,5-dimethoxybenzaldehyde **3** afforded the benzylic alcohol **4** in 95% yield. Oxidation of alcohol **4** with PCC provided ketone **5**, which was demethylated with molten pyridinium chloride, affording the dihydroxyphenyl-dodecyl ketone **6** in 14% overall yield. Finally, the acid-catalyzed condensation of phenyl ketone **6** with pyrrole afforded, after column chromatography, purification, and crystallization from acetonitrile, the calixpyrrole-resorcinarene hybrid **2b** as a white solid in 19% yield.

As shown in Figure 2, the ^{1}H NMR spectrum of **2b** in $CDCl_3$ solution shows broad proton signals. We assume that similarly to the reported findings for **2c** this is mainly due to aggregation

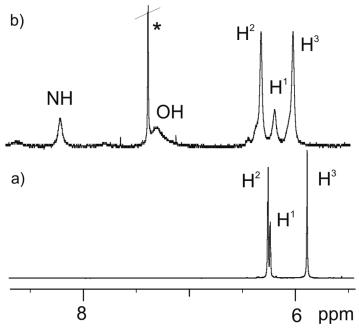

Figure 2. Selected downfield region of ^{1}H NMR spectra of 10 mM solutions of calixpyrrole **2b** (a) in MeOH-d_4 and (b) in $CDCl_3$. *Residual peak of nondeuterated solvents. See Scheme 1 for proton assignment.

phenomena. Conversely, in polar organic solvents that disrupt intermolecular hydrogen-bonding interactions, such as MeOH-d_4 or THF-d_8, the ^{1}H NMR spectrum of **2b** shows sharp and well-defined proton signals.

Scheme 1. Synthetic Scheme for the Preparation of the Calix[4]pyrrole-Resorcin[4]arene hybrid 2b

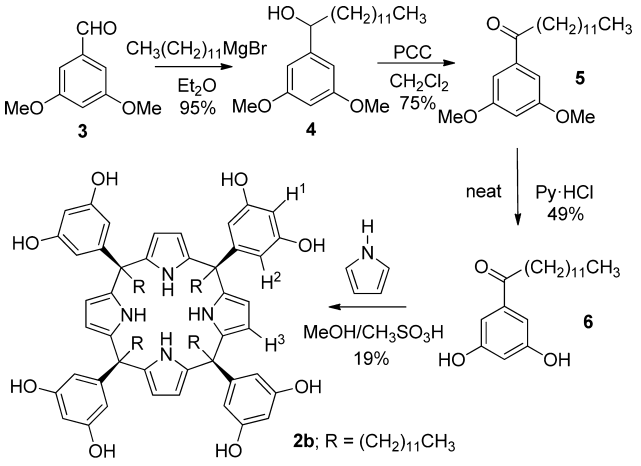

Single crystals of **2b** suitable for X-ray diffraction were grown from an acetonitrile solution. The analysis of the diffraction data revealed that in the solid state calixpyrrole **2b** adopts the cone conformation and features one molecule of acetonitrile included in its aromatic cavity (Figure 3). The cone conformation of **2b** is stabilized by the formation of intramolecular hydrogen bonds between the hydroxyl groups at its upper rim. In addition, the included acetonitrile molecule is hydrogen-bonded simultaneously to the four convergent pyrrolic NHs of **2b**. The binding geometry of the solvate $CH_3CN\subset$**2b** is a key factor in stabilizing the calix[4]pyrrole core in the cone conformation. The averaged N···N distance of the four hydrogen bonds is 3.22 Å. The acetonitrile solvate $CH_3CN\subset$**2b** packs into rows through the intermediacy of water molecules that are hydrogen-bonded to two adjacent solvates in the same row.

The *meso*-alkyl substituents (tails) belonging to adjacent $CH_3CN\subset$**2b** complexes are involved in van der Waals interactions. Each row of $CH_3CN\subset$**2b** solvate is flanked by two analogous parallel rows with the polar upper rims (head) of **2b** oriented in opposite directions. This arrangement of rows forms a layer with alternating lipophilic and hydrophilic strips.

dx.doi.org/10.1021/jo5007224 | J. Org. Chem. 2014, 79, 5545−5557

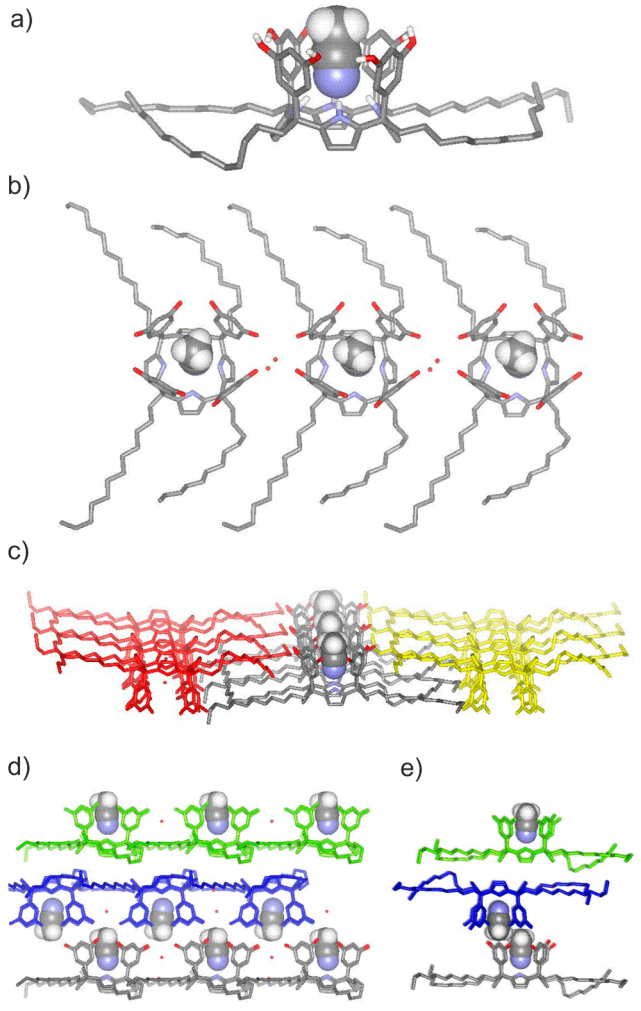

Figure 3. (a) X-ray structure of the solvate $CH_3CN\subset$**2b**; (b) adjacent solvates of $CH_3CN\subset$**2b** form rows; (c) three rows of adjacent $CH_3CN\subset$**2b** solvates pack to form a layer with the polar heads oriented in opposite directions; (d) side and (e) front views of the bilayers resulting from the packing of layers of solvates. For clarity, nonpolar hydrogen atoms are removed in panel a and all hydrogen atoms are removed in panels b–d. Selected acetonitrile molecules are shown as CPK models, and **2b** is depicted in stick representation.

Layers pack on top of each other by confronting strips of the same polarity. Thus, head-to-head interactions between $CH_3CN\subset$**2b** solvates in different layers are promoted through water-mediated hydrogen-bonding interactions, whereas tail-to-tail contacts are mainly of van der Waals nature. Each molecule of **2b** is involved in head-to-head interactions with two other molecules of **2b** pertaining to two contiguous rows of an adjacent layer. Acetonitrile molecules fill the voids produced in the described packing. The crystal packing demonstrates the existence of bilayers of calixpyrrole molecules **2b**, in which the polar and nonpolar sections segregate. This result highlights the amphiphilic character of **2b**.

Synthesis of Calix[4]pyrrole-Based Deep Cavitands. The construction of deep cavitands based on resorcin[4]arene **1** relies in the elaboration of its aromatic cavity by incorporation of four aromatic flaps at its upper rim. The additional aromatic flaps are easily introduced through nucleophilic aromatic substitution reactions between the hydroxyl groups at the upper rim of **1** and *ortho*-disubstituted fluoro and chloro electron-deficient six-membered aromatic and heteroaromatic rings.[28]

Using analogous synthetic procedures to the ones applied for the elaboration of the cavity of **1**, we set out to synthesize deep cavitands derived from the calix[4]pyrrole-resorcin[4]arene hybrid **2b**. The reaction of hybrid **2b** with 4 equiv of *o*-1,2-difluoro-4,5-dinitrobenzene **7** carried out by heating a dimethylformamide (DMF) solution at 85 °C in the presence of an excess of triethylamine afforded, after column chromatography purification, the four-folded bridged cavitand **8** as a yellow solid (mp >251 °C, decomp) in 47% yield. We did not detect the presence of partially (reacted) bridged products in the reaction mixture.

Similarly, the reaction of **2b** with 1,2-difluoro-4,5-dicyano benzene **9** produced octanitrile calix[4]pyrrole cavitand **10** as a white solid (mp >292 °C, decomp) in 69% yield (Scheme 2).

The synthesis of cavitands **12** and **14** required the modification of the reaction conditions. Thus, **2b** was reacted with 4 equiv of 2,3-dichloroquinoxaline **11** using potassium carbonate as a base in DMF. After purification of the crude reaction, cavitand **12** was isolated as a white solid in 51% yield (mp >328 °C, decomp). Analogously, the reaction of 2,3-dichloro-1,4-pyrazine **13** with **2b** afforded cavitand **14** as a white solid (mp >275 °C, decomp) in 12% yield.

Structures of the Vase and Kite Conformers of Calix[4]-pyrrole-Based Deep Cavitands, Thermodynamic Stabilities, and Interconversion Processes. Molecular modeling studies indicate that in cavitands **8**, **10**, **12**, and **14** the base of four phenyl rings, which are connected at the *meso* positions of the calix[4]pyrrole unit, and the four 15-membered rings formed an enforced concave cavity closed at one end by the four pyrrole rings. Regardless of the starting geometry assigned to the calix[4]pyrrole core of the four cavitands, the energy minimized structure always converged to a cone conformation. In short, it was not possible to energy minimize any of these cavitands with the calix[4]pyrrole core exhibiting 1,2- or 1,3-alternate conformations. The energy minimized models showed that the four phenyl bridging groups attached at the upper rims of **8** and **10**, the diazanaphthalenes of **12**, and the four 1,3-pyrazine units in **14** resemble flaps that can adopt axial (a) or equatorial (e) orientations. Consequently and in close analogy to the cavitands derived from resorcin[4]arene **1**,[29] we expected that cavitands **8**, **10**, **12**, and **14** could also adopt kite and vase conformations. The structures of the new cavitands in both conformations were energy minimized using MM3 (see Figure 4 for cavitand **10** including one molecule of DMF).

The MM3 energy minimized vase (a,a,a,a) conformer of the calix[4]pyrrole cavitands possess C_{4v}-like symmetry. In this conformation, the fixed aromatic cavity defined by the *meso*-phenyl substituents is significantly increased by the four bridging aromatic panels. For example, in the energy minimized structure of the vase conformer of **10** one molecule of DMF and one molecule of chloroform could be included in its deep aromatic cavity (Figure 4a). The MM3 energy minimized kite structures of the cavitands also displayed C_{4v}-like symmetry. As shown for the kite conformer of **10** (Figure 4b) the lone pairs of the eight oxygen atoms are outwardly directed with respect to its fixed aromatic cavity. Using the MM3 force field as implemented in the Scigress Program,[30] the energy difference for the two conformers of **10** containing one DMF molecule included in their aromatic cavity is 12.7 kcal/mol more favorable as the kite.

dx.doi.org/10.1021/jo5007224 | J. Org. Chem. 2014, 79, 5545–5557

Scheme 2. Synthetic Scheme for the Preparation of Deep Cavitands 8, 10, 12, and 14

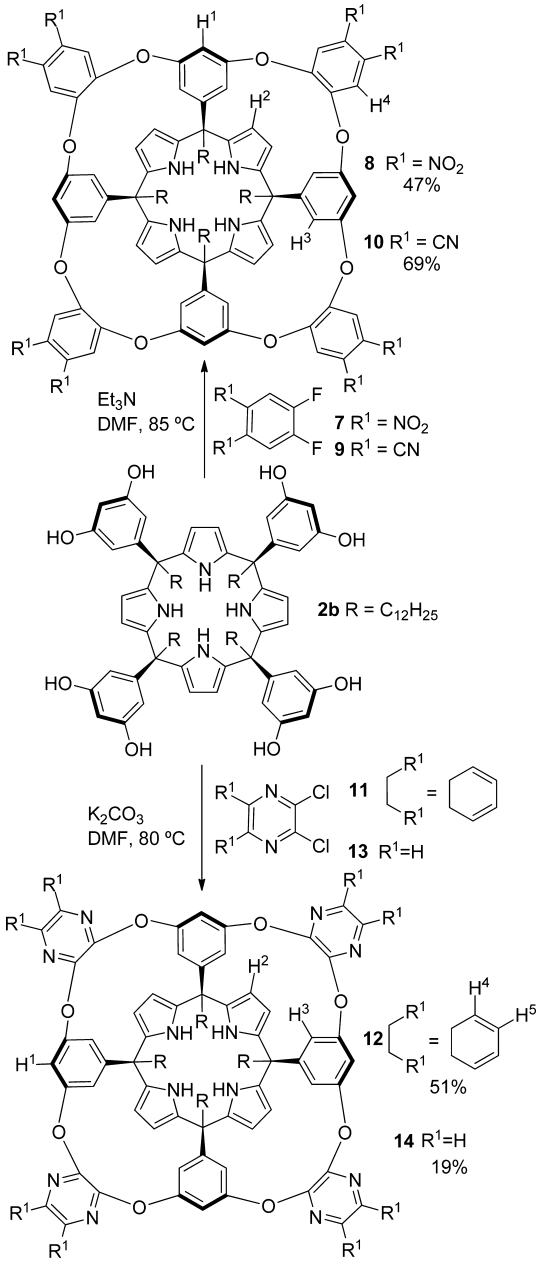

We computed the energy difference between the empty vase and kite conformers of **10** at the BP86[31,32]-D3[33]/def2-SVP level of theory using TURBOMOLE version 6.4.[34] C_4 symmetry restrictions were imposed on both structures in order to speed up the calculation time. Interestingly, the energy minimized kite conformer of **10** with C_4 symmetry featured the lone pairs of four of the eight oxygen atoms inwardly directed with respect to the aromatic cavity, representing an example of an inherently chiral concave molecule (Figure 5).[35] The cyclochiral conformer shown in Figure 5 is defined to have *M* axial chirality assuming that the oxygen atom with the inwardly directed lone pair takes priority over the one having outwardly directed lone pairs.[36,37] This structure is reminiscent of the kite conformation of resorcinarene cavitands; however, in this latter case they exhibited C_{2v} symmetry.[1,2] At this level of theory, the energy difference between the inclusion complexes

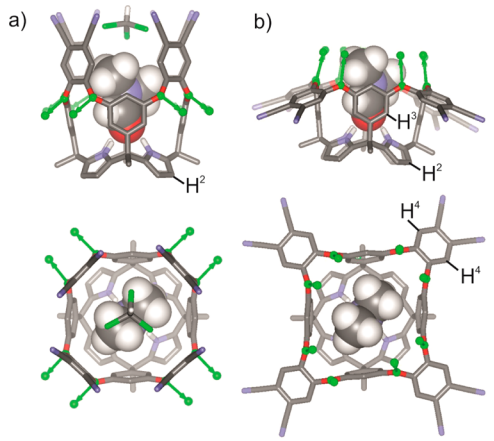

Figure 4. Side and top views of the MM3 energy minimized structures of (a) vase (a,a,a,a) conformer of cavitand **10** modeled with one molecule of DMF (shown as CPK model) and one molecule of chloroform (stick representation) included in its cavity, and (b) kite (e,e,e,e) conformer with C_{4v}-like symmetry. Nonpolar hydrogen atoms are omitted for clarity. The kite conformer is modeled with just one molecule of DMF included. The average orientation of the lone pairs on the oxygen atoms (Lp) in the two structures is indicated by green vectors included in the plane defined by the Lp1-oxygen atom-Lp2 and bisecting the angle they define.

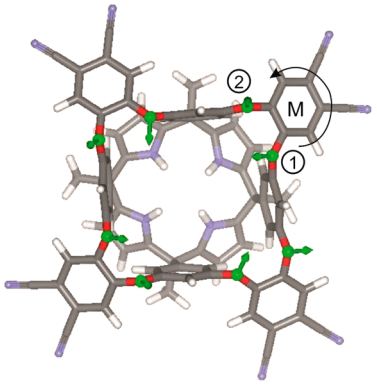

Figure 5. Energy-minimized structure of the kite conformer of **10** displaying C_4 symmetry at the BP86-D3/def2-SVP level of theory.

of 4-phenyl-pyridine-*N*-oxide **17** with the vase and kite conformers of **10** is 8 kcal/mol in favor of the kite (see Supporting Information). Taken in concert, the results of the theoretical calculations indicated that cavitand **10** should adopt exclusively the kite conformation, displaying either C_{4v} or C_4 symmetry. A reverse trend of energies was computed for the two forms of the inclusion complex of the same *N*-oxide and the pyrazine-based cavitand **17**⊂**14** (ΔE = 8.8 kcal/mol in favor of the vase) (Supporting Information). Moreover, diazanaphthalene cavitand **12** shows a significant energy preference for the vase form of the inclusion complex with phenylpyridine *N*-oxide, **17**⊂**12** (ΔE = 22 kcal/mol in favor of the vase) (Supporting Information).

The ^{1}H NMR spectra of the deep cavitands **10**, **12**, and **14** taken in different solvents (CD_2Cl_2, toluene-d_8) and at different temperatures (−60 to 100 °C) show sharp proton signals, the number of which is consistent with a C_{4v} symmetry. The signals do not experience substantial changes in their chemical shifts and shapes as the temperature is changed. At room temperature and in $CDCl_3$ solutions the *β*-pyrrolic protons (H^2) of the

dx.doi.org/10.1021/jo5007224 | J. Org. Chem. 2014, 79, 5545−5557

aromatic bridged cavitands resonate at $\delta \approx 5.7$ ppm (see Scheme 2 and Figure 4 for proton assignment). Thus, they appear upfield ($\Delta\delta = -0.32$ ppm) from the β-pyrrolic protons (H^2) of the conformationally rigid methylene bridged cavitand **15** (Figure 6) that resonate at $\delta = 6.02$ ppm. In addition, the

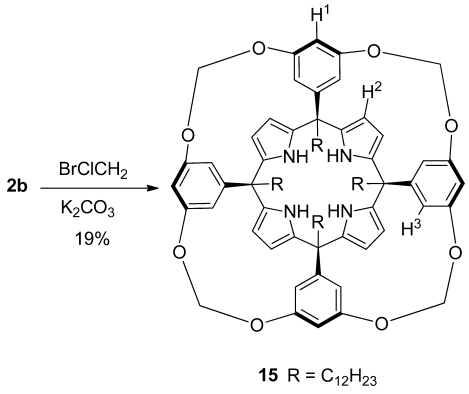

Figure 6. Synthetic scheme of the methylene bridged cavitand **15**.

doublet of the H^3 protons in the resorcinol units of the aryl bridged cavitands ($\delta = 5.84$, 5.87, 5.76, and 5.54 ppm for **8**, **10**, **12**, and **14**, respectively) are also shifted upfield ($\Delta\delta \approx -0.4$–0.7 ppm) with respect to the same signal in **15** ($\delta = 6.3$ ppm). In short, the β-pyrrolic protons H^2 and the aromatic protons H^3 in cavitands **8**, **10**, **12**, and **14** must be close to the shielding cone exerted by the bridging aromatic ring. In sum, these NMR observations suggest that in solution and in the range of studied temperatures the aromatic bridged cavitands are locked in the kite (e,e,e,e) conformation, a result that is not in agreement with the theoretical calculations discussed above.

Moreover, a kite conformer displaying C_{4v} symmetry would explain the reduced number of proton signals observed in the ^{1}H NMR spectra. However, the putative existence of a chemical exchange process (cycloenantiomerization) between two cyclochiral C_4 kite conformers that is fast on the ^{1}H NMR chemical shift time scale at any of the investigated temperatures (213–378 K) could also explain the absence of signal splitting for diastereotopic protons, i.e., H^4 and $H^{4\prime}$, which can be expected for a kite structure with C_4 symmetry (Figure 7).

Luckily, single crystals of cavitands **8**, **10**, and **12** suitable for X-ray diffraction analysis grew from separate solutions of acetonitrile or acetonitrile/dichloromethane mixtures. In the three cases, the cavitands, in the solid state, adopted a kite conformation with C_4 symmetry having one molecule of solvent included in their fixed aromatic cavites: DMF for **10** and CH_3CN for **8** and **12**. The solvent molecule is hydrogen-bonded simultaneously to the four pyrrole N–H hydrogen atoms, and the calix[4]pyrrole core adopts a cone conformation (Figure 7).

For the three different cavitands, as could be expected, the two cyclochiral (*M* and *P*) enantiomers of the C_4 kite conformer are present in the packing of the lattice. Most likely, in solution the kite structures of the cavitands are also C_4 symmetric, but the two cyclochiral conformers are rapidly interconverting on the ^{1}H NMR time scale (Scheme 3).

The structure of the transition state for the cycloenantiomerization process was investigated by means of theoretical calculations at the BP86-D3/def2-SVP level of theory for the interconversion between the cyclochiral conformers of the octacyano cavitand **10** (see Supporting Information). The

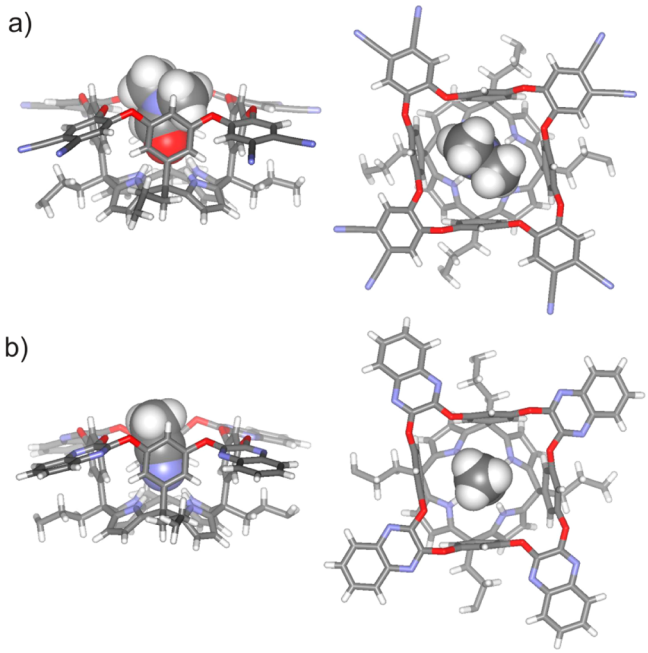

Figure 7. Side and top views of the X-ray structures of the C_4 kite conformer of cavitands: (a) DMF⊂**10** and (b) CH_3CN⊂**12**. Only the *M* cyclochiral conformer is shown, and the length of the *meso*-alkyl groups is truncated to three methylenes for clarity. The cavitands are displayed in stick representation, and the included solvent molecules are shown as CPK models.

energy of the transition state lies just 0.9 kcal/mol higher than the C_4 kite ground state of the cyclochiral conformers. The structure of the transition state is similar to that of a kite conformer with C_{4v} symmetry obtained in the energy minimization runs using MM3 (Figure 4b and Supporting Information). The low energy barrier computed for the transition state suggests that it is not possible to induce a slow exchange interconversion process on the NMR time scale by lowering the temperature. Consequently, in agreement with experiment, the diastereotopic protons H^4 and $H^{4\prime}$ (see Scheme 2 and Scheme 3 for proton assignment) of the C_4 kite conformers are observed as one signal.

Molecular Recognition Studies of Pyridine N-oxide Derivatives by Calix[4]pyrrole-Based Deep Cavitands. Attempts To Change the Relative Thermodynamic Stabilities of the Vase and Kite Forms by Guest Inclusion. Pyridine *N*-oxides are important targets for molecular recognition studies due to their pronounced biological activity.[38,39] We reported that aryl extended calix[4]pyrroles[40] and their supramolecular capsular derivatives[41–43] bind pyridine *N*-oxides and other aromatic and aliphatic *N*-oxides with high affinity. The oxygen atom of the *N*-oxide forms four simultaneous hydrogen bonds with the pyrrole NHs of the calix[4]pyrrole core. The *N*-oxide guests are bound deep in the aromatic cavity of the host and experience additional CH–π and π–π intermolecular interactions with the *meso*-aryl substituents. On the basis of our previous findings, we decided to investigate the interaction of the calix[4]pyrrole deep cavitands synthesized in this work with a series of pyridine *N*-oxides (Figure 8).

We first probed the binding of the *N*-oxides by these cavitands in $CDCl_3$ solution using ^{1}H NMR spectroscopy. The addition of 0.5 equiv of 4-dimethylaminopyridine *N*-oxide **16** to a 1 mM $CDCl_3$ solution of octanitro cavitand **8** resulted in two

dx.doi.org/10.1021/jo5007224 | J. Org. Chem. 2014, 79, 5545–5557

Scheme 3. Cycloenantiomerizaton Equilibrium between the Two Cyclochiral *M* and *P* Kite C_4 Conformers of 8[a]

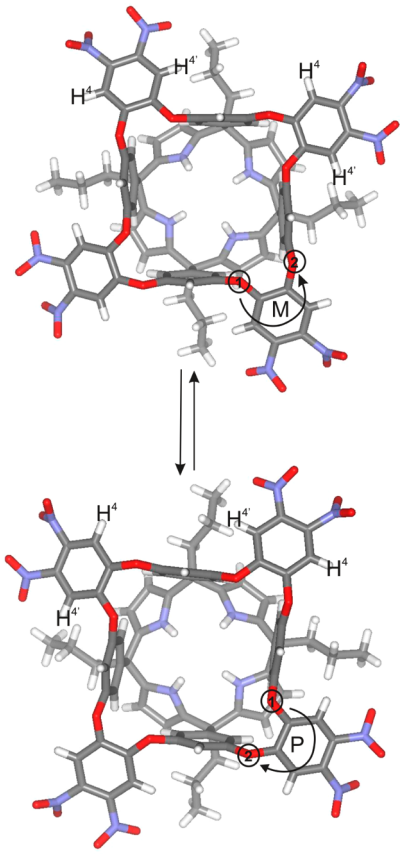

[a]The structures of the two cyclochiral enantiomers were extracted from the packing of the X-ray structure of the crystal. The *meso*-alkyl groups are truncated to three carbons for clarity. In solution the interconversion process is fast on the ^{1}H NMR chemical shift time scale and the diasterotopic protons H^4 and $H^{4'}$ resonate as one signal even at temperatures below 220 K.

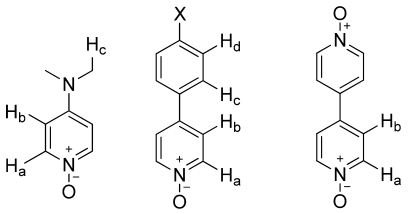

Figure 8. Molecular structures of the pyridine *N*-oxide derivatives used in this work.

sets of signals of equal intensity for the protons of the host (Figure 9). The two sets of signals belong to the protons of free and bound host **8**, indicating that the chemical exchange process is slow on the ^{1}H NMR time scale. The large downfield shift ($\Delta\delta$ = 1.29 ppm) observed for the pyrrole NHs of bound **8** is indicative of the formation of hydrogen bonds with the oxygen atom of the bound *N*-oxide **16**. Protons H^2, H^3, and H^4 of host **8** experience reduced changes of their chemical shifts with respect to the free state, while H^1 shifts slightly upfield ($\Delta\delta$ = −0.23 ppm). This effect is probably due to the shielding

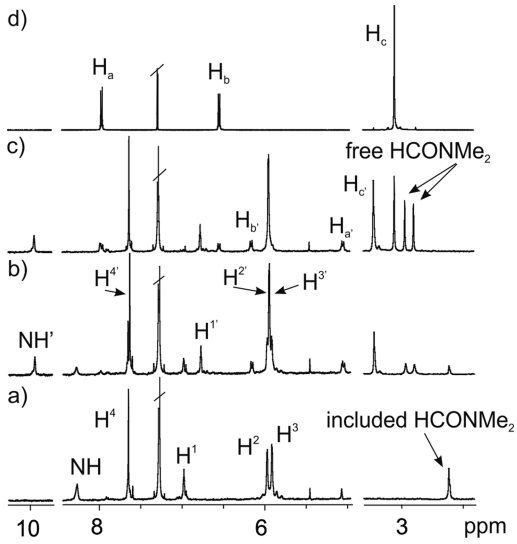

Figure 9. Selected region of ^{1}H NMR spectra acquired during the titration of a 1 mM $CDCl_3$ solution of cavitand **8** with incremental amounts of DMAP *N*-oxide **16**: (a) 0 equiv, (b) 0.5 equiv, and (c) 1.5 equiv. (d) ^{1}H NMR spectra of free *N*-oxide **16** in $CDCl_3$ solution. Primed letters and numbers indicate protons in the **16**⊂**8** complex. See Scheme 2 and Figure 8 for proton assignments.

effect of the bound *N*-oxide. The signals assigned to the aromatic protons of bound **16** moved upfield (H_a $\Delta\delta$ = −3.13 ppm and H_b $\Delta\delta$ = −0.42 ppm), supporting the inclusion of the *N*-oxide in the fixed aromatic cavity of **8**. In the presence of 1 equiv of **16** only the proton signals assigned to the bound host and the bound guest were detected. This observation indicates the quantitative formation of a 1:1 complex, **16**⊂**8**, for which a stability constant value larger than 10^4 M^{-1} can be estimated. The addition of an excess of **16** did not induce any change in the chemical shifts of the protons assigned to the 1:1 complex. However, signals for the protons of free **16** became visible in the ^{1}H NMR spectrum of the mixture. A 2D-EXSY experiment performed on a 1 mM solution of cavitand **8** containing 1.5 equiv of *N*-oxide **16** revealed the absence of cross peaks between the signals of the free and bound *N*-oxide. This result shows that the exchange rate between the free and bound *N*-oxide is too slow to be measured with this technique and suggests that the **16**⊂**8** complex is kinetically very stable (>5 s).

It is worth noting that the incremental addition of *N*-oxide **16** to a $CDCl_3$ solution of **8** induced the emergence and subsequent growth of the proton signals characteristic for DMF. We rationalized this observation assuming that cavitand **8** is isolated as a DMF solvate. The DMF molecule is included in the cavity of **8** and is bound to the four pyrrole NHs through the oxygen atom (see X-ray structure of **10** in Figure 10). The included DMF could not be removed even after heating a sample of **8** for 24 h under high vacuum conditions. Most likely, the octanitro cavitand **8** binds *N*-oxide **16** considerably stronger than DMF, inducing the exchange of guests and the release of free DMF to the bulk solution. The exchange of a bound DMF molecule by the included *N*-oxide is observed in all titration experiments performed with the cavitand series. The elemental analysis of the yellow solid isolated as cavitand **8** is in agreement with the presence of one molecule of DMF for each cavitand.

The minimal chemical shift changes observed for the H^2 and H^3 protons of **8** upon binding suggest that in the **16**⊂**8**

dx.doi.org/10.1021/jo5007224 | J. Org. Chem. 2014, 79, 5545−5557

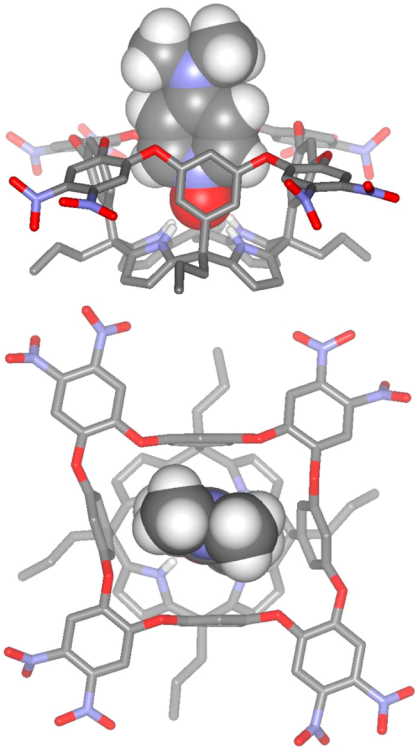

Figure 10. Side and top views of the X-ray structure of the **16⊂8** complex. Nonpolar hydrogen atoms of **8** are removed, and alkyl chains are pruned for clarity. *N*-Oxide **16** is shown as CPK model, and **8** is in stick representation.

complex the cavitand maintains the kite conformation. Single crystals of the **16⊂8** complex suitable for X-ray diffraction grew from the $CDCl_3$ solution. The solid state structure of the **16⊂8** complex is in complete agreement with that assigned in solution based on the observed chemical shift changes. In the crystal, the bound octanitro cavitand **8** is in the kite form with the calix[4]pyrrole core in the cone conformation displaying an overall C_4-like symmetry. The oxygen atom of the bound *N*-oxide **16** is hydrogen-bonded to the four pyrrole NHs. The aromatic protons, alpha to the nitrogen atom, are included in the fixed aromatic cavity of **8**. The pyridyl group of the *N*-oxide experiences simultaneous $\pi-\pi$ and CH$-\pi$ interactions with the *meso*-aryl walls of the cavitand.

Completely analogous results were obtained in the titration of octacyano cavitand **10** with 4-dimethylaminopyridine *N*-oxide **16**.

After the addition of 1 equiv of DMAP *N*-oxide **16** to a 1 mM $CDCl_3$ solution of cavitand **12**, the formation of a 1:1 inclusion complex was observed in the ^{1}H NMR spectrum. The large downfield shift of the pyrrolic NHs ($\Delta\delta$ = 1.59 ppm) and the upfield shift of the protons for the included guest clearly support the formation of the inclusion complex **16⊂12**. In contrast with the titration results obtained for the previous cavitands, **8** and **10**, the formation of the 1:1 inclusion complex between the DMAP *N*-oxide **16** and the tetradiazanaphthalene cavitand **12** generated a reduced upfield shift for the H^1 proton ($\Delta\delta$ = −0.08 ppm for **16⊂12** vs −0.23 ppm **16⊂8** and **16⊂10**). Concomitantly, the H^3 proton of bound cavitand **12** moved downfield ($\Delta\delta$ = 0.15 ppm). The chemical shift of the H^3 proton in cavitands **8** and **10** was almost unaffected upon *N*-oxide binding. These unparalleled chemical shift changes observed for the H^1 and H^3 protons in the titration of tetradiazanaphthalene cavitand **12** with **16** suggested to us the possible existence of a conformational switch of the diazanaphthalene flaps, from the axial to equatorial position, induced by the binding of the *N*-oxide. That is, the **16⊂12** complex could exist in solution as an undetermined mixture of vase and kite forms of the cavitand involved in a fast chemical exchange on the ^{1}H NMR time scale.

To further explore the putative complexation induced conformational switch of **12**, we decided to use 4-phenylpyridine-*N*-oxide **17** as a guest. Our expectations were that the *p*-phenyl substituent of *N*-oxide **17** should favor the formation of the **17⊂12** complex in vase form. On the one hand, the phenyl substituent is shape and size complementary to the additional aromatic cavity present in the vase conformer of **12** compared to the kite. Additionally, the vase conformer of complex **17⊂12** should be energetically favored by additional $\pi-\pi$ and CH$-\pi$ interactions established between the *p*-phenyl substituent of **17** and the diazanaphthalene flaps in the axial conformation (Figure 11). As expected, the interaction of

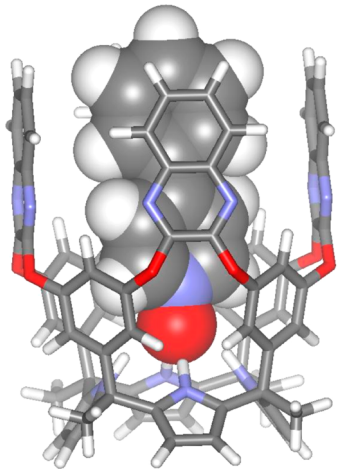

Figure 11. MM3 energy minimized structure of the putative **17⊂12** complex in the vase form.

phenyl *N*-oxide **17** with cavitand **12** featured a slow chemical exchange process on the ^{1}H NMR time scale. The ^{1}H NMR analysis of an equimolar mixture of **17** and **12** in $CDCl_3$ solution revealed the quantitative formation of the **17⊂12** complex. Unexpectedly, the magnitude of the downfield shift experienced by the H^3 proton in the **17⊂12** complex ($\Delta\delta$ = 0.15 ppm) was coincident with the one observed for inclusion of the shorter *N*-oxide **16**. This result constituted an indication of the failure to provoke a notable guest-induced switch of the kite to the vase form in the inclusion complex **17⊂12**.

In addition, the signals of the protons pertaining to the *p*-phenyl substituent of included **17** did not shift noticeably with respect to those of the free *N*-oxide. To evaluate if the modification of the electronic properties of the *p*-phenyl ring of the pyridine *N*-oxide had any effect on the possible conformational switch of the bound cavitand **12**, we prepared 4-(4-methoxyphenyl)pyridine *N*-oxide **18** and 4-(4-nitrophenyl)-pyridine *N*-oxide **19** (Figure 8). Both pyridine *N*-oxide derivatives produced 1:1 complexes with **12**. The stability constant values for these complexes can be estimated to be larger than 10^4 M^{-1} in $CDCl_3$ solution. In the case of the methoxy-*N*-oxide **18**, the signal of the H^3 proton of **12** in the inclusion complex **18⊂12** shifts upfield 0.14 ppm, a value that

dx.doi.org/10.1021/jo5007224 | J. Org. Chem. 2014, 79, 5545−5557

coincides with the one observed for the **17⊂12** complex. Interestingly, the upfield shift experienced by the H^3 proton in the **19⊂12** complex with the nitro *N*-oxide is larger, 0.21 ppm. Additionally, the signal of the *ortho* protons of the *p*-nitrophenyl ring of **19** in the latter complex move somewhat upfield ($\Delta\delta$ = −0.23 ppm). Taken together, these results suggest that in solution the nitro *N*-oxide **19** is capable of inducing a kite to vase conformational switch of the bound cavitand **12** to a larger, although undetermined, extent than the other pyridine *N*-oxide derivatives **17** and **18**. In contrast with these findings, the analysis of the X-ray diffraction data of single crystals of complexes **17⊂12**, **18⊂12**, and **19⊂12** revealed that, in the solid state, cavitand **12** exclusively adopts the kite form in the three inclusion complexes (Supporting Information).

Pyridine *N*-oxides **18** and **19** were also used to investigate the putative guest-induced conformational switch using the shorter aryl bridged cavitands **10** and **14**. The obtained results point to exclusive formation of inclusion complexes in which the shorter cavitands are in the kite form (Supporting Information).

Tetramethylene bridged cavitand **15** is deprived of aromatic flaps and constitutes an ideal reference to determine the expected chemical shift changes for the protons of the host induced by the inclusion of *N*-oxides. The equimolar mixture of methylene bridged cavitand **15** and 4-phenylpyridine *N*-oxide **17** in $CDCl_3$ solution at 1 mM concentration produced the quantitative formation of the **17⊂15** complex. The ^{1}H NMR spectrum of the mixture indicated that, in response to guest inclusion, the H^1 proton in **15** moves upfield ($\Delta\delta$ = −0.53 ppm). Most likely, the observed chemical shift change is due to the shielding effect produced by the *p*-phenyl group of the included *N*-oxide. In addition, the chemical shift values of protons H^2 and H^3 in **15** are insensitive to the inclusion process. These results provide strong support to the hypothesis that the detected changes in chemical shifts for equivalent protons in cavitand **12** are indeed caused by a conformational change in the aromatic flaps.

We wanted to evaluate the effect of temperature in the kite to vase conversion of cavitand **12** when involved in the formation of inclusion complexes with *N*-oxides. It is known that in related cavitands derived from a resocin[4]arene scaffold, the vase form is favored at high temperatures owing to an increase in the negative entropic term over the positive enthalpy component of the kite to vase conversion.[44] The variable temperature experiments were performed in solutions of tetrachloroethane-d_2, a solvent with a boiling point of 146 °C. In this solvent and at 298 K, the chemical shift changes experienced by the protons of the complexes between cavitand **12** and the series of pyridine *N*-oxides **17**, **18**, and **19** were similar to those observed in $CDCl_3$ solution.

Increasing the temperature to 398 K amplifies the chemical shift changes. For the three inclusion complexes, the downfield shift experienced by H^3 in bound **12** increases 2-fold. Similarly, the upfield shift of the *ortho*-proton, H_c, in the phenyl substituent of the included *N*-oxides doubles its magnitude. Taken in concert, these data suggest that the increase in temperature favors the vase form of the cavitand **12** in the inclusion complexes. Unfortunately, the available data do not allow the determination of an accurate percentage of kite and vase forms of the cavitand in these complexes at different temperatures.

Similar variable temperature experiments performed with an equimolar mixture of the shorter tetrapyrazine cavitand **14** and methoxyphenyl *N*-oxide **18** revealed that in the **18⊂14** complex the chemical shifts of protons H^3 and H_c are not modified by temperature changes. This result underlines a clear conformational preference for the kite form in bound cavitand **14**. This is in contrast to the observations made with related pyrazine cavitands based on resocin[4]arene scaffolds, which are locked in the vase form.[2]

From the results obtained in the ^{1}H NMR titration experiments, the stability constants of the 1:1 inclusion complexes formed between cavitands, **8**, **10**, **12**, and **14**, and pyridine *N*-oxide derivatives, **16**, **17**, **18**, **19**, and **20**, were estimated to be larger than 10^4 M^{-1} (quantitative formation of the 1:1 complex in the presence of equimolar amounts of host and guest at mM concentration). For this reason, we undertook the calculation of accurate values for the stability constants of these 1:1 complexes using isothermal titration calorimetry (ITC) experiments. The ITC data obtained for the titrations of designated cavitands (**12** and **10**) with phenylpyridine *N*-oxide **17** displayed double sigmoid curves. Figure 12 displays the plot of the normalized integrated heat (black diamonds) vs molar ratio [**17**]/[**12**] for the titration of **12** with phenyl-*N*-oxide **17**.

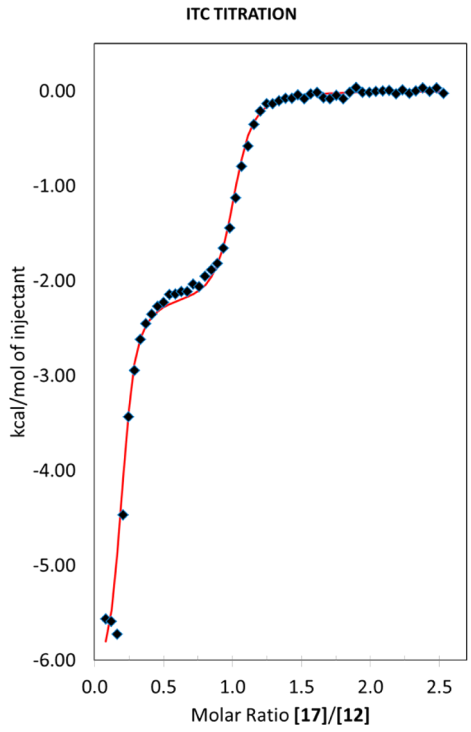

Figure 12. Plot of the normalized integration heat (black diamonds) vs [**17**]/[**12**] molar ratio obtained for the ITC experiment of **12** (0.99 mM) with **17** (9.8 mM) in $CHCl_3$. Theoretical binding isotherm (red line) for a binding model that considers three species, **12**, DMF, and **17**, and two complexes, DMF⊂**12** and **17⊂12**, fit to the experimental data is also shown.

The two inflection points of the double sigmoid binding isotherm are centered at values close to 0.25 and 1 for the molar ratio [**17**]/[**12**]. ITC dilution experiments performed on both the cavitand and the pyridine *N*-oxide showed insignificant release of heat. In addition, a DOSY NMR experiment carried out with a $CDCl_3$ solution containing a 2:1 mixture of cavitand **12** and phenyl *N*-oxide **17** provided similar diffusion coefficient values for the free and bound cavitand. These findings ruled out the existence of dimerization/

dx.doi.org/10.1021/jo5007224 | J. Org. Chem. 2014, 79, 5545−5557

oligomerization processes for **12** or **17** in solution in the range of used concentrations. As we already commented above, the solid isolated as cavitand **12** was in fact, to a great extent, a DMF solvate of **12**. On the basis of this precedent and using the HypDH software, we were able to fit the double sigmoid binding curve to a theoretical binding model that considers the existence of three species and five stoichiometric states: free **12**, free DMF, free **17**, DMF⊂**12**, and **17**⊂**12** (Figure 12). The concentration of DMF in the calorimetric cell was determined to be 0.85 × [**12**].[45] In short, only 15% of the molecules in the solid isolated as **12** do not include a molecule of DMF. The fit of the ITC data returned the values of ΔH(DMF⊂**12**) = −4.1 kcal/mol, ΔH(**17**⊂**12**) = −6.3 kcal/mol, K(DMF⊂**12**) = 5.5 × 10^5 M^{-1} and K(**17**⊂**12**) = 6.3 × 10^7 M^{-1}. The 2 orders of magnitude difference measured for the stability constants of the complexes of **12** indicates the almost exclusive formation of the **17**⊂**12** complex when DMF and *N*-oxide **17** are in solution in an equimolar ratio with respect to **12**. The speciation profiles derived from the ITC experiments are in complete agreement with the observations made in the ^{1}H NMR titrations of **12** with **17** (release of approximately 1 equiv of DMF to the bulk solution on addition of 1 equiv of **17**). We attempted to remove the DMF from the solid isolated as cavitand **12** by continuous heating under high vacuum. However, the ITC experiments performed with samples of **12** treated as indicated above also produced double-sigmoid binding curves with reduced changes in the molar ratio of the first inflection point. The deep inclusion of DMF in the conformationally rigid aromatic cavity of **12** means that its release is energetically highly disfavored because it produces an empty cavity (vacuum). The deep inclusion nature of complexes **17**⊂**12** and DMF⊂**12** is also responsible of the favorable entropic terms (3.3 and 3.7 kcal/mol, respectively) determined for their complexation processes. Both host and guest must experience strong desolvation processes prior to the formation of the inclusion complex. The release of solvating chloroform molecules to the bulk solution assists binding entropically, even in such a nonpolar solvent, overcoming the loss of translational and rotational entropy of one of the partners and of the conformational flexibility of host and guest bound in the complex.

We decided to grade the stability constant values of some inclusion complexes of cavitands **12** and **10** with designated phenyl-*N*-oxides by performing pairwise competitive experiments and analyzing them using ^{1}H NMR spectroscopy. An equimolar mixture of cavitand **12** with phenyl-*N*-oxide **17** and methoxyphenyl-*N*-oxide **18** in $CDCl_3$ produced inclusion complexes **17**⊂**12** and **18**⊂**12** in an exact 1:1 ratio, demonstrating that the stability constant values of the two complexes are independent of the electronic nature of the *p*-phenyl substituent of the *N*-oxide. We also performed a pairwise competitive experiment by mixing equimolar amounts of cavitands **10** and **12** with methoxyphenyl- *N*-oxide **18**. The obtained $CDCl_3$ solution was analyzed by ^{1}H NMR spectroscopy indicating the formation of complexes **18**⊂**10** and **18**⊂**12** in equal amounts. This latter result proves that the stability constants of the caviplexes resulting from calix[4]pyrrole cavitands **10** and **12** and pyridine *N*-oxides are not significantly influenced by the characteristics of the bridging aromatic ring.

The preference exhibited by cavitand **12** to adopt the kite form in the inclusion complexes with pyridine *N*-oxides prompted us to investigate the formation of three-component aggregates involving one molecule of a bis-*N*-oxide (ditopic guest) and two units of cavitand **12**. Molecular modeling studies indicate that 4,4′-dipyridyl-*N*,*N*′-dioxide **20** is a suitable molecular platform to study such assembly process. The energy minimized structure of the complex **20**⊂**12**$_2$ did not show clear signs of attractive or repulsion interactions between the two units of **12** (Figure 13).

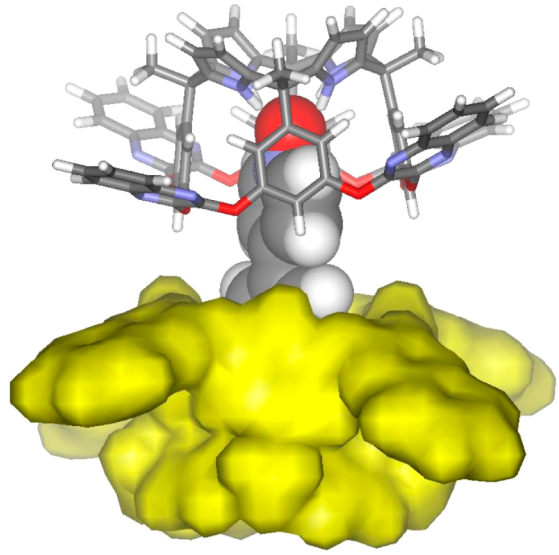

Figure 13. Energy-minimized structure of the **20**⊂**12**$_2$ complex. One unit of **12** is depicted in stick representation, the other is shown as a van der Waals surface, and the bis-*N*-oxide **20** is shown as a CPK model.

The binding of bis-*N*-oxide **20** with **12** was probed in $CDCl_3$ solution using ^{1}H NMR spectroscopy. Addition of 0.25 equiv of bis-*N*-oxide **20** resulted in the appearance of a new set of signals (Figure 14b). We assigned the new signals to the protons of the

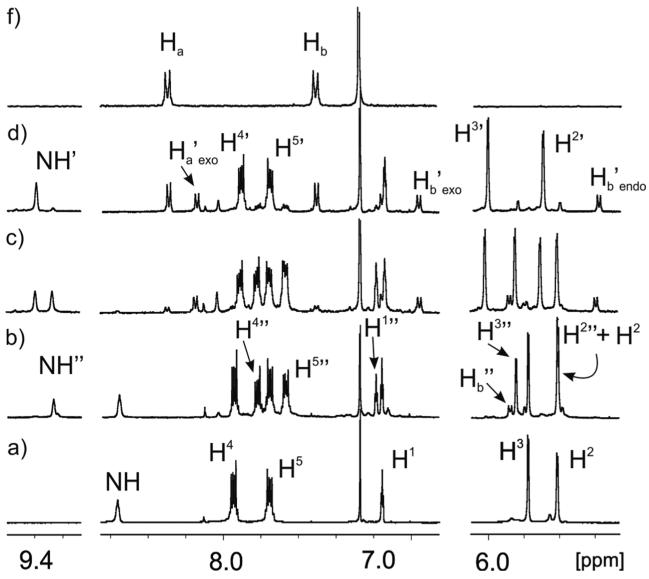

Figure 14. Selected regions of the ^{1}H NMR spectra acquired during the titration of a 1 mM $CDCl_3$ solution of tetradiazanaphthalene cavitand **12** with bis *N*-oxide **20**. Equivalents added: (a) 0, (b) 0.25, (c) 0.75, (d) 1.5. (f) The same regions of the ^{1}H NMR spectrum of **20**. Primed letters and numbers indicate protons in the **20**⊂**12** complex, and doubly primed correspond to the **20**⊂**12**$_2$ complex.

dx.doi.org/10.1021/jo5007224 | J. Org. Chem. 2014, 79, 5545−5557

cavitand **12** in the **20⊂12**$_2$ complex. The pyrrole NHs of the cavitand in the 1:2 complex resonate downfield at δ = 9.27 ppm, indicating the formation of hydrogen bonds with the oxygen atom of bound **20**. The protons of bound **20** appear highly upfield shifted: δ = 5.82 and 7.68 ppm for H_a'' and H_b'', respectively, and as a unique set. These observations are in agreement with the inclusion of each binding site of **20** in one unit of **12** producing a 1:2 complex, **20⊂12**$_2$, featuring D_{4h}-like symmetry.

In the presence of 0.5 equiv of bis-*N*-oxide **20** we observed the emergence of a new set of proton signals for **12** that do not correspond with those assigned to the free host or the 1:2 complex. These signals must correspond to a new inclusion complex in which the pyrrole NHs resonate at δ = 9.40 ppm. Upon further addition of **20**, the intensity of the signals of the latter complex grew at the expenses of those of **20⊂12**$_2$ (Figure 14c,d). Interestingly, the protons of bound **20** in the new complex resonate as four separate signals. Two of them appear at chemical shift values that are in line with those observed for the included *N*-oxide in the **20⊂12**$_2$ complex. The other two, however, are just slightly upfield shifted with respect to the protons in free **20**. The relative integrals for these four signals are 1:1:1:1. When 0.75 equiv of **20** is added, the signals for the protons of free *N*-oxide start to arise. In the presence of 1.5 equiv of **20** the **20⊂12** complex is the major species in solution. Taken together, these observations indicate that the incremental addition of **20** induces the destruction of the **20⊂12**$_2$ complex and induces the formation of a new 1:1 complex, **20⊂12**. The observation of four proton signals for the included *N*-oxide in the **20⊂12** complex is consistent with its lower symmetry. The determination of accurate values for the stability constants of the 1:1 complex from the ^{1}H NMR titration data is hampered by the large value of the microscopic binding constants ($K_m > 10^4$ M^{-1}) assigned to the interaction of the pyridine *N*-oxide group with the cavitand **12**. Nevertheless, after all of the free cavitand is consumed, it is possible to determine an average value for the equilibrium constant of the destruction process K_d (eq 1 in Scheme 4) by integrating the signals assigned to the **20⊂12** and **20⊂12**$_2$ complexes in the presence of different amounts of **20**.

Scheme 4. Equilibria Involved in the Destruction of the 20⊂12$_2$ Complex (1) and in the Formation of the 20⊂12 (2) and 20⊂12$_2$ (3) Complexes[a]

$$\mathbf{20}\subset\mathbf{12}_2 + \mathbf{20} \overset{K_d}{\rightleftharpoons} 2 \bullet \mathbf{20}\subset\mathbf{12} \qquad K_d = \frac{[\mathbf{20}\subset\mathbf{12}]^2}{[\mathbf{20}\subset\mathbf{12}_2]\,[\mathbf{20}]} \quad (1)$$

$$\mathbf{12} + \mathbf{20} \rightleftharpoons \mathbf{20}\subset\mathbf{12} \qquad K_{1:1} = 2K_m \quad (2)$$

$$\mathbf{20}\subset\mathbf{12} + \mathbf{20} \rightleftharpoons \mathbf{20}\subset\mathbf{12}_2 \qquad K_{1:1\leftrightarrow 1:2} = \alpha K_m/2 \quad (3)$$

$$K_d = \frac{K_{1:1}}{K_{1:1\leftrightarrow 1:2}} = 4/\alpha \quad (4)$$

[a]The relationship of the equilibrium constants with K_m (microscopic constant), α (the cooperativity factor), and statistical correction factors are shown (4).

Using the relationship that exists between K_d and the cooperativity factor (α) of the *N*-oxide **20** (eq 3 in Scheme 4), we determined α to be 0.09. A value of $\alpha < 1$ for **20** indicates the existence of a negative cooperativity in the assembly process of the **20⊂12**$_2$ complex. In other words, the second binding event (3) leading to the formation of the **20⊂12**$_2$ complex from the preformed **20⊂12** is less favorable than the statistical estimate derived from the microscopic constant value of the first binding event. Most likely, the binding of the second unit of **12** is disfavored by a combination of electrostatic and steric effects. On one hand, the upfield shift observed for the protons of the diazanaphthalene flaps in the **20⊂12**$_2$ complex suggest their involvement in $\pi-\pi$ stacking interactions between adjacent units of **12**. On the other hand, the reduced downfield shift experienced by the pyrrole NHs in the **20⊂12**$_2$ complex compared to those in **20⊂12** points to the formation of larger hydrogen bonds in the latter. This can be either a consequence of repulsive interactions between the two units of **12** in the **20⊂12**$_2$ complex or to a modification of negative density of the free oxygen atom of the *N*-oxide in the **20⊂12** complex. The existence of a negative cooperativity in the assembly of the **20⊂12**$_2$ complex is also supported by the observation of a solution mixture of free **12**, **1:1**, and **1:2** complexes when working under strict stoichiometric control (ratio of [**20**]/[**12**] = 0.5).

CONCLUSIONS

We report here the synthesis of a novel family of deep cavitands based on a calix[4]pyrrole scaffold. The cavitands have been characterized both in the solid state and in solution. Whereas resorcinarene-based cavitands easily switch between the vase and the kite conformations with temperature, the calix[4]-pyrrole-derived cavitands are conformationally more rigid than their resorcinarene analogues. In the range of conditions studied they are locked in a C_4 kite form as a racemic mixture of two cycloenantiomers. Molecular modeling studies are in agreement with the experimental observations. The energy barrier calculated for the interconversion between cycloenantiomers is very low (0.9 kcal/mol), explaining the fast interconversion observed in solution. Pyridine *N*-oxide derivatives are included by the deep cavitands yielding 1:1 caviplexes that are thermodynamically and kinetically highly stable. The putative conformational switch between the kite and vase forms of the calix[4]pyrrole cavitands was studied using variable temperatures ^{1}H NMR experiments and by including *N*-oxide guests that are size and shape complementary to the vase form. The obtained results suggest that only the cavitand decorated with four diazanaphthalene flaps undergoes such conformational switching when complexed with an electron-poor pyridine *N*-oxide derivative and at elevated temperature. The extent of the conformational switch could not be determined, but the magnitude of the observed chemical shift changes suggest that it is reduced. Finally, the complexation of the ditopic bipyridine bis-*N*-oxide **20** with cavitand **12** produced the formation of the 1:2 complex through a noncooperative binding process.

EXPERIMENTAL SECTION

Methods and Materials. ^{1}H NMR and ^{13}C NMR spectra were recorded on a 400 and 500 MHz spectrometer. All solvents were dried prior to use. 1,2-Difluoro-4,5-dinitrobenzene was prepared according to a reported procedure.[46] 4,5-Difluorophthalonitrile and 2,3-dichloroquinoxaline were commercially available and used without further purification.

Synthesis of 4. To an oven-dried 100 mL round-bottomed flask containing magnesium turnings (1.46 g, 60 mmol) was added dry ether (15 mL) under argon atmosphere. Bromododecane (7.5 mL, 30 mmol) was added dropwise through a dropping funnel over 30 min under reflux. From the last addition, the reaction was kept under reflux for a further 45 min, then a solution of 3,5-dimethoxybenzaldehyde (5

dx.doi.org/10.1021/jo5007224 | J. Org. Chem. 2014, 79, 5545−5557

g, 30 mmol) in dry ether (25 mL) was added dropwise, and the mixture was left to react for an additional 3 h. The reaction was quenched by addition of a saturated solution of NH_4Cl (35 mL). The collected organic layers were washed with water and brine and dried over sodium sulfate. The solvent was removed under reduced pressure, affording 9.5 g (95% yield) of a white solid that was used without further purification. ^{1}H NMR (400 MHz, $CDCl_3$): δ 6.50 (d, J = 2.3 Hz, 2H), 6.37 (t, J = 2.3 Hz, 1H), 3.79 (s, 6H), 2.93 (t, J = 7.6 Hz, 2H), 1.72 (m, 2H), 1.21−1.33 (m, 18H), 0.87 (t, J = 6.5 Hz, 3H). HRMS-ESI+ m/e calcd for $C_{21}H_{35}O_2$ $(M - OH)^+$ 319.2637, found 319.2641

Synthesis of 5. In a 250 mL round-bottomed flask filled with dry dichloromethane (40 mL) were added pyridinium chlorochromate (3.84 g, 17.8 mmol), silica (3.84 g), and alcohol **4** (2g, 5.9 mmol) in one portion. The reaction mixture was stirred at rt for 2 h, then diluted with ether, and filtered over a bed of Celite (1 cm) and silica (3 cm). The filtrate was concentrated under reduced pressure, and the residue was recrystallized from methanol, affording 1.5 g (75% yield) of a white crystalline solid. ^{1}H NMR (500 MHz, $CDCl_3$, 298 K): δ 7.09 (d, J = 2.4 Hz, 2H), 6.64 (t, J = 2.4 Hz, 1H), 3.84 (s, 6H), 2.91 (t, J = 7.6 Hz, 2H), 1.71 (m, 2H), 1.21−1.39 (m, 18H), 0.87 (t, J = 6.8 Hz, 3H). HRMS-ESI+ m/e calcd for $C_{21}H_{35}O_3$ $(M + H)^+$ 335.2586, found 335.2585

Synthesis of 6. In a 10−20 mL microwave vial, ketone **5** (1g, 3 mmol) and pyridinium chloride (3.45 g, 30 mmol) were irradiated at 250 °C for 1 h. The residue was partitioned between water and ethyl acetate. The aqueous layer was extracted three times with ethyl acetate. The combined organic layers were dried over sodium sulfate, and the solvent was removed under reduced pressure. Recrystallization of the residue afforded 452 mg (49% yield) of **6** as white solid. ^{1}H NMR (400 MHz, $CDCl_3$, 298 K): δ 6.99 (d, J = 2.3 Hz, 2H), 6.54 (t, J = 2.3 Hz, 1H), 2.87 (m, 2H), 1.69 (m, 2H), 1.23−1.33 (m, 18H), 0.87 (t, J = 6.7 Hz, 3H). HRMS-ESI$^-$ m/e calcd for $C_{19}H_{29}O_3$ $(M - H)^-$ 305.2117, found 305.2115

Synthesis of Octahydroxy Calixpyrrole 2b. To a 100 mL round-bottomed flask containing a solution of pyrrole (0.25 mL, 3.6 mmol) in MeOH (6 mL) was added methanesulfonic acid (0.24 mL, 10.77 mmol) dropwise. The mixture was stirred for 5 min, then a solution of ketone **6** (1.1 g, 3.6 mmol) in MeOH (18 mL) was added slowly, and the reaction was left at rt overnight protected from light. The reaction was quenched by addition of water (30 mL) and extracted with ethyl acetate (4 × 50 mL). The combined organic layers were dried over sodium sulfate, and the solvent was removed under reduced pressure. The mixture crude was purified by chromatography (SiO_2; dichloromethane/ethyl acetate from 8:2 to 6:4) affording a brownish solid that was recrystallized from acetonitrile (245 mg, 19% yield). ^{1}H NMR (500 MHz, MeOD, 25 °C): δ 8.89 (bs, 4H), 6.18 (d, J = 2.0 Hz, 8H), 6.15 (t, J = 2.0 Hz, 4H), 5.89 (d, J = 2.4 Hz, 8H), 2.30 (m, 8H), 1.35 (m, 74H), 0.89 (t, J = 7.0 Hz, 12H); ^{13}C NMR ($CDCl_3$/100 MHz): δ 157.0, 148.5, 137.2, 108.4, 104.9, 100.6, 40.1, 38.1, 31.8, 30.2, 29.6, 29.55, 29.50, 29.48, 29.2, 25.22, 22.45, 13.21 HRMS-MALDI+ m/z calculated for $C_{92}H_{132}N_4O_8Na$ 1443.9942, found 1443.9937. Mp > 142 °C (decomp)

Synthesis of Octanitrocalix[4]pyrrole 8. A mixture of octahydroxycalix[4]pyrrole (145 mg, 0.102 mmol) and 1,2-difluoro-4,5-dinitrobenzene (91 mg, 0.445 mmol) was placed in an oven-dried Schlenk flask and dried under vacuum for 10 min. Dry DMF (15 mL) was added under argon, and while stirring, triethylamine (distilled over calcium hydride, 0.136 mL, 0.972 mmol) was added dropwise. The flask was heated to 85 °C overnight. The reaction was concentrated under reduced pressure, and the residue was purified by column chromatography (silica gel, dichloromethane/hexane 6:4) to give product **8** (100 mg, yield 47%) as a yellowish solid that can be recrystallized from acetonitrile. ^{1}H NMR ($CDCl_3$/400 MHz): δ 8.33 (bs, 4H), 7.66 (s, 8H), 6.93 (t, J = 2.0 Hz, 4H), 5.85 (d, J = 2.2 Hz, 8H) 5.79 (d, J = 2.0 Hz, 8H), 2.17 (m, 8H), 1.36−1.13 (m, 80H), 0.88 (t, J = 6.2 Hz, 12H); ^{13}C NMR ($CDCl_3$/100 MHz): δ 158.2, 153.0, 150.4, 140.2, 135.2, 120.9, 110.9, 110.5, 106.6, 48.9, 32.0, 29.9, 29.8, 29.7, 29.6, 29.5, 29.4, 22.7, 14.1. MS-MALDI− m/e calcd for $C_{116}H_{132}N_{12}O_{24}$ 2076.95, found 2076.8. Anal. Calcd for $C_{116}H_{132}N_{12}O_{24}$·DMF: C, 66.43; H, 6.51; N, 8.46. Found: C, 66.82; H, 6.28; N, 8.49. Mp > 251 °C (decomp).

Synthesis of Octanitrilecalix[4]pyrrole 10. In a sealed tube the octahydroxycalix[4]pyrrole (200 mg, 0.141 mmol) and 4,5-difluorophthalonitrile (99 mg, 0.605 mmol) were dissolved in 5 mL of dry DMF. Triethylamine (distilled over calcium hydride, 0.196 mL, 1.406 mmol) was added, and the tube was heated to 85 °C overnight. The reaction was concentrated under reduced pressure, and the residue was purified by column chromatography (silica gel, dichloromethane) and recrystallized from acetonitrile to afford **9** (186 mg, yield 69%) of an off-white solid. ^{1}H NMR ($CDCl_3$/500 MHz): δ 8.33 (bs, 4H), 7.52 (s, 8H), 6.93 (t, J = 2.4 Hz, 4H), 5.87 (d, J = 2.6 Hz, 8H) 5.70 (d, J = 2.4 Hz, 8H), 2.17 (m, 8H), 1.37−1.24 (m, 80H), 0.90 (t, J = 6.3 Hz, 12H); ^{13}C NMR ($CDCl_3$/100 MHz): δ 158.4, 152.7, 151.2, 135.3, 129.3, 114.2, 113.8, 110.2, 106.2, 105.8, 48.8, 39.3, 37.6, 32.0, 30.0, 29.9, 29.8, 29.7, 29.6, 29.5, 29.4, 25.6, 22.8, 14.2. HRMS-MALDI m/z calculated for $C_{124}H_{132}N_{12}O_8$ 1917.0291, found 1917.0286. Mp > 292 °C (decomp).

Synthesis of Tetraquinoxaline 12. In a sealed tube were placed the octahydroxycalix[4]pyrrole (500 mg, 0.352 mmol), 2,3-dichloroquinoxaline (361 mg, 1.758 mmol) and dry potassium carbonate (486 mg, 3.52 mmol). Ten milliliters of dry DMF was added, and the tube was heated to 85 °C overnight. HCl 1 N (10 mL) was added, and the precipitate was filtered under vacuum. Purification of the solid by column chromatography (silica gel, dichloromethane) and recrystallization from acetonitrile afforded **12** as a white solid (345 mg, yield 51%). ^{1}H NMR ($CDCl_3$/500 MHz): δ 8.59 (bs, 4H), 7.95 (dd, J_1 = 3.4 Hz, J_2 = 6.2 Hz, 8H), 7.76 (dd, J_1 = 3.4 Hz, J_2 = 6.2 Hz 8H), 7.16 (t, J = 2.0 Hz, 4H), 5.78 (d, J = 2.0 Hz, 8H), 5.61 (d, J = 2.0 Hz, 8H), 2.04 (m, 8H), 1.38−1.12 (m, 80H) 0.92 (t, J = 6.1 Hz, 12H); ^{13}C NMR ($CDCl_3$/100 MHz): δ 157.7, 150.9, 149.4, 139.7, 135.7, 129.9, 127.9, 111,9, 106.9, 105.2, 48.5, 39.3, 37.8, 31.9, 30.7, 30.2, 30.0, 29.9, 29.9, 29.8, 29.7, 29.4, 24.7, 22.7, 14.1. MS-MALDI+ m/e calcd for $C_{124}H_{140}N_{12}O_8$ 1925.1, found 1925.0 Anal. Calcd for $C_{124}H_{140}N_{12}O_8$·DMF: C, 76.28; H, 7.41; N, 9.11. Found: C, 76.08; H, 7.36; N, 9.14. Mp > 328 °C (decomp).

Synthesis of Tetrapyrazine Cavitand 14. In a sealed tube were placed the octahydroxycalix[4]pyrrole (305 mg, 0.214 mmol), 2,3-dichloropyrazine (118 μL, 1.072 mmol) and dry potassium carbonate (296 mg, 2.145 mmol). Ten milliliters of dry DMF was added, the tube was heated to 85 °C overnight, 10 mL of HCl 1 N was added, and the precipitate was filtered under vacuum. Purification of the solid by column chromatography (silica gel, dichloromethane/THF 98:2) and recrystallization from acetonitrile afforded **14** as a white solid (45 mg, yield 12%). ^{1}H NMR ($CDCl_3$/500 MHz): δ 8.19 (bs, 8H), 8.12 (s, 4H), 7.00 (t, J = 2.2 Hz, 4H), 5.70 (d, J = 2.5 Hz, 8H), 5.54 (d, J = 2.2 Hz, 8H), 2.04 (m, 8H), 1.38−1.12 (m, 80H) 0.88 (t, J = 6.5 Hz, 12H); ^{13}C NMR ($CDCl_3$/100 MHz): δ 157.9, 150.9, 140.2, 135.7, 111.0, 106.1, 105.2, 48.61, 31.9, 30.0−29.3, 22.7, 14.1. Mp > 275 °C (decomp). HRMS-ESI+ m/e calcd for $C_{108}H_{132}N_{12}O_8$ $(M + Na)^+$ 1748.0189, found 1748.0188.

Synthesis of Tetramethylene Bridged Cavitand 15. In a 25 mL oven-dried Schlenk tube were placed the octahydroxycalixpyrrole **2b** (21 mg, 0.015 mmol) and oven-dried potassium carbonate (24 mg, 0.174 mmol), and the contents were dried under high vacuum for 3 h. Then, under argon, 1.2 mL of dry DMF was added. The flask was heated to 85 °C, and then bromochloromethane (50 μL, 0.769 mmol) was added in one portion. The flask was heated for an additional 3 h. The reaction was concentrated under reduced pressure and purified by column chromatography (silica gel, dichlorometane/hexane 1:1 to pure dichloromethane) to afford the product as a white solid (4 mg, yield 18%). ^{1}H NMR ($CDCl_3$/500 MHz): δ 7.46 (bs, 4H), 6.46 (t, J = 2.1 Hz, 4H), 6.38 (d, J = 2.1 Hz, 8H), 6.10 (d, J = 7.6 Hz, 4H), 6.02 (d, J = 2.6 Hz, 8H), 5.37 (d, J = 7.6 Hz, 4H), 2.35 (m, 8H), 1.38−1.12 (m, 80H), 0.90 (t, J = 6.9 Hz, 12H); ^{13}C NMR ($CDCl_3$/100 MHz): δ 156.6, 149.8, 136.9, 109.1, 108.3, 105.4, 87.9, 48.8, 38.9, 31.9, 30.2, 29.7, 29.6, 29.5, 29.3, 25.1, 22.7, 14.1. HRMS-ESI+ m/e calcd for $C_{96}H_{132}N_4O_8$ $(M + Na)^+$ 1491.9943, found 1491.9920.

Synthesis of 4-(4-Methoxyphenyl)pyridine *N*-Oxide 18. In a 100 mL round bottomed flask, the 4-methoxy(4-phenyl)pyridine (150

dx.doi.org/10.1021/jo5007224 | J. Org. Chem. 2014, 79, 5545−5557

mg, 0.810 mmol) was dissolved in 20 mL of dry chloroform. Then, mCPBA was added in small portions (300 mg, 1.215 mmol). After 2.5 h of stirring at room temperature, an extra portion of mCPBA was added (200 mg). After 1 h the reaction was concentrated and eluted through a column of basic alumina, first with dichloromethane and finally with dichloromethane/methanol 9:1 until elution of the pure product as a hygroscopic yellow solid (130 mg, 80% yield). ^{1}H NMR ($CDCl_3$/500 MHz): δ 8.26 (d, J = 7.2 Hz, 2H), 7.54 (d, J = 8.9 Hz, 2H), 7.48 (d, J = 7.2 Hz, 2H), 7.01 (d, J = 8.9 Hz, 2H), 3.87 (s, 3H); ^{13}C NMR ($CDCl_3$/400 MHz): δ 160.6, 139.2, 139.0, 128.3, 127.6, 123.0, 114.76, 55.4. HRMS-ESI+ m/e calcd for $C_{12}H_{12}NO_2$ ($M + H^+$) 202.0868, found 202.0863

Synthesis of 4-(4-Nitrophenyl)pyridine *N*-Oxide 19. In a 50 mL round bottomed flask, the 4-nitro(4-phenyl)pyridine (22 mg, 0.109 mmol) was dissolved in 10 mL of water and 10 mL of 2-butanone. Then, sodium bicarbonate was added (276 mg, 3.28 mmol), and the mixture was stirred vigorously. Oxone was added in small portions (202 mg, 0.328 mmol), and the reaction was stirred at room temperature for 3 h. Then 50 mL of brine was added, and the reaction was extracted three times with chloroform. The organic layers are combined, dried over sodium sulfate, and concentrated under reduced pressure to afford the *N*-oxide as yellow needles (20 mg, yield 85%). ^{1}H NMR ($CDCl_3$/500 MHz): δ 8.37 (d, J = 8.3 Hz, 2H), 8.32 (d, J = 6.1 Hz, 2H), 7.77 (d, J = 8.3 Hz, 2H), 7.57 (d, J = 6.1 Hz, 2H); ^{13}C NMR ($CDCl_3$/100 MHz): δ 160.5, 139.2, 139.1, 128.3, 127.6, 123.0, 114.7. HRMS-ESI− m/e calcd for $C_{11}H_9N_2O_3$ 217.0613, found 217.0618

■ ASSOCIATED CONTENT

Supporting Information

^{1}H and ^{13}C NMR spectra of the synthesized compounds, ^{1}H NMR spectra registered during the variable temperature experiments, ^{1}H NMR spectra acquired in the binding studies, fits of the ITC titration data, figures of the X-ray crystal structures discussed in the text but not shown in the manuscript, and X-ray crystallographic files of **2b**, **8**, **10**, **12**, **16⊂8**, **17⊂12**, **18⊂12**, and **19⊂12**. This material is available free of charge via the Internet at http://pubs.acs.org.

■ AUTHOR INFORMATION

Corresponding Author

*E-mail: pballester@iciq.es.

Notes

The authors declare no competing financial interest.

■ ACKNOWLEDGMENTS

We thank Gobierno de España MINECO (CTQ2011-23014), Generalitat de Catalunya DURSI (2009SGR6868,) and ICIQ Foundation for financial support. A.G. thanks MINECO for a FPU fellowship. A.F. thanks DIGYT of Spain (projects CTQ2011-27512/BQU and CONSOLIDER INGENIO 2010 CSD2010-00065, FEDER funds) for financial support. We also thank Professor Shannon Biros from the Chemistry Department of the Grand Valley State University, Allendale, Michigan for editing this manuscript.

■ REFERENCES

(1) Moran, J. R.; Karbach, S.; Cram, D. J. *J. Am. Chem. Soc.* **1982**, *104*, 5826−5828.
(2) Moran, J. R.; Ericson, J. L.; Dalcanale, E.; Bryant, J. A.; Knobler, C. B.; Cram, D. J. *J. Am. Chem. Soc.* **1991**, *113*, 5707−5714.
(3) Dalcanale, E.; Soncini, P.; Bacchilega, G.; Ugozzoli, F. *J. Chem. Soc., Chem. Commun.* **1989**, 500−502.
(4) Soncini, P.; Bonsignore, S.; Dalcanale, E.; Ugozzoli, F. *J. Org. Chem.* **1992**, *57*, 4608−4612.
(5) Rieth, S.; Hermann, K.; Wang, B. Y.; Badjic, J. D. *Chem. Soc. Rev.* **2011**, *40*, 1609−1622.
(6) Rudkevich, D. M.; Rebek, J. *Eur. J. Org. Chem.* **1999**, 1991−2005.
(7) Korner, S. K.; Tucci, F. C.; Rudkevich, D. M.; Heinz, T.; Rebek, J. *Chem.—Eur. J.* **2000**, *6*, 187−195.
(8) Heinz, T.; Rudkevich, D. M.; Rebek, J. *Nature* **1998**, *394*, 764−766.
(9) Liu, X. J.; Warmuth, R. *J. Am. Chem. Soc.* **2006**, *128*, 14120−14127.
(10) Biavardi, E.; Tudisco, C.; Maffei, F.; Motta, A.; Massera, C.; Condorelli, G. G.; Dalcanale, E. *Proc. Natl. Acad. Sci. U.S.A.* **2012**, *109*, 2263−2268.
(11) Gissot, A.; Rebek, J. *J. Am. Chem. Soc.* **2004**, *126*, 7424−7425.
(12) Pochorovski, I.; Ebert, M. O.; Gisselbrecht, J. P.; Boudon, C.; Schweizer, W. B.; Diederich, F. *J. Am. Chem. Soc.* **2012**, *134*, 14702−14705.
(13) Pochorovski, I.; Boudon, C.; Gisselbrecht, J. P.; Ebert, M. O.; Schweizer, W. B.; Diederich, F. *Angew. Chem., Int. Ed.* **2012**, *51*, 262−266.
(14) Renslo, A. R.; Rebek, J. *Angew. Chem., Int. Ed.* **2000**, *39*, 3281−3283.
(15) Hooley, R. J.; Restorp, P.; Iwasawa, T.; Rebek, J. *J. Am. Chem. Soc.* **2007**, *129*, 15639−15643.
(16) Xiao, S. X.; Ajami, D.; Rebek, J. *Chem. Commun.* **2010**, *46*, 2459−2461.
(17) Lucking, U.; Rudkevich, D. M.; Rebek, J. *Tetrahedron Lett.* **2000**, *41*, 9547−9551.
(18) Gale, P. A.; Sessler, J. L.; Kral, V.; Lynch, V. *J. Am. Chem. Soc.* **1996**, *118*, 5140−5141.
(19) Anzenbacher, P.; Jursikova, K.; Lynch, V. M.; Gale, P. A.; Sessler, J. L. *J. Am. Chem. Soc.* **1999**, *121*, 11020−11021.
(20) Gil-Ramirez, G.; Benet-Buchholz, J.; Escudero-Adan, E. C.; Ballester, P. *J. Am. Chem. Soc.* **2007**, *129*, 3820−3821.
(21) Ciardi, M.; Tancini, F.; Gil-Ramirez, G.; Escudero-Adan, E. C.; Massera, C.; Dalcanale, E.; Ballester, P. *J. Am. Chem. Soc.* **2012**, *134*, 13121−13132.
(22) Lippmann, T.; Wilde, H.; Dalcanale, E.; Mavilla, L.; Mann, G.; Heyer, U.; Spera, S. *J. Org. Chem.* **1995**, *60*, 235−242.
(23) Jacopozzi, P.; Dalcanale, E.; Spera, S.; Chrisstoffels, L. A. J.; Reinhoudt, D. N.; Lippmann, T.; Mann, G. *J. Chem. Soc., Perkin Trans. 2* **1998**, 671−677.
(24) Dionisio, M.; Oliviero, G.; Menozzi, D.; Federici, S.; Yebeutchou, R. M.; Schmidtchen, F. P.; Dalcanale, E.; Bergese, P. *J. Am. Chem. Soc.* **2012**, *134*, 2392−2398.
(25) Delangle, P.; Mulatier, J. C.; Tinant, B.; Declercq, J. P.; Dutasta, J. P. *Eur. J. Org. Chem.* **2001**, 3695−3704.
(26) Melegari, M.; Suman, M.; Pirondini, L.; Moiani, D.; Massera, C.; Ugozzoli, F.; Kalenius, E.; Vainiotalo, P.; Mulatier, J. C.; Dutasta, J. P.; Dalcanale, E. *Chem.—Eur. J.* **2008**, *14*, 5772−5779.
(27) Slovak, S.; Evan-Salem, T.; Cohen, Y. *Org. Lett.* **2010**, *12*, 4864−4867.
(28) Purse, B. W.; Rebek, J. *Proc. Natl. Acad. Sci. U.S.A.* **2005**, *102*, 10777−10782.
(29) Moran, J. R.; Ericson, J. L.; Dalcanale, E.; Bryant, J. A.; Knobler, C. B.; Cram, D. J. *J. Am. Chem. Soc.* **1991**, *113*, 5707−5714.
(30) *SCIGRESS V 3.0.0*; Fujitsu Limited: Tokyo, 2014; http://www.fujitsu.com/global/services/solutions/tc/hpc/app/scigress/.
(31) Becke, A. D. *Phys. Rev. A* **1988**, *38*, 3098−3100.
(32) Perdew, J. P. *Phys. Rev. B* **1986**, *33*, 8822−8824.
(33) Grimme, S.; Antony, J.; Ehrlich, S.; Krieg, H. *J. Chem. Phys.* **2010**, *132*, 154104.
(34) Ahlrichs, R.; Bär, M.; Häser, M.; Horn, H.; Kölmel, C. *Chem. Phys. Lett.* **1989**, *162*, 165−169.
(35) Szumna, A. *Chem. Soc. Rev.* **2010**, *39*, 4274−4285.
(36) Szumna, A. *Org. Biomol. Chem.* **2007**, *5*, 1358−1368.
(37) Buckley, B. R.; Boxhall, J. Y.; Page, P. C. B.; Chan, Y. H.; Elsegood, M. R. J.; Heaney, H.; Holmes, K. E.; McIldowie, M. J.; McKee, V.; McGrath, M. J.; Mocerino, M.; Poulton, A. M.; Sampler, E. P.; Skelton, B. W.; White, A. H. *Eur. J. Org. Chem.* **2006**, 5117−5134.

(38) Stevens, M.; Pannecouque, C.; De Clercq, E.; Balzarini, J. *Biochem. Pharmacol.* **2006**, *71*, 1122−1135.
(39) Balzarini, J.; Stevens, M.; Andrei, G.; Snoeck, R.; Strunk, R.; Pierce, J. B.; Lacadie, J. A.; De Clercq, E.; Pannecouque, C. *Helv. Chim. Acta* **2002**, *85*, 2961−2974.
(40) Verdejo, B.; Gil-Ramirez, G.; Ballester, P. *J. Am. Chem. Soc.* **2009**, *131*, 3178−3179.
(41) Espelt, M.; Ballester, P. *Org. Lett.* **2012**, *14*, 5708−5711.
(42) Gil-Ramirez, G.; Chas, M.; Ballester, P. *J. Am. Chem. Soc.* **2010**, *132*, 2520−2521.
(43) Adriaenssens, L.; Ballester, P. *Chem. Soc. Rev.* **2013**, *42*, 3261−3277.
(44) Roncucci, P.; Pirondini, L.; Paderni, G.; Massera, C.; Dalcanale, E.; Azov, V. A.; Diederich, F. *Chem.—Eur. J.* **2006**, *12*, 4775−4784.
(45) The ratio 0.85:1 established between the concentrations of DMF and **12** was derived from manually fitting the value of the molar ratio for the inflexion point in the first sigmoidal curve.
(46) Kazimierczuk, Z.; Dudycz, L.; Stolarski, R.; Shugar, D. *J. Carbohydr., Nucleosides, Nucleotides* **1981**, *8*, 101−117.